

# Dynamic Proxy Domain Generalizes the Crowd Localization by Better Binary Segmentation

Junyu Gao<sup>1</sup>, Member, IEEE, Da Zhang<sup>1</sup>, and Xuelong Li<sup>1</sup>, Fellow, IEEE

**Abstract**—Crowd localization targets on predicting each instance precise location within an image. Current advanced methods propose the pixel-wise binary classification to tackle the congested prediction, in which the pixel-level thresholds binarize the prediction confidence of being the pedestrian head. Since the crowd scenes suffer from extremely varying contents, counts and scales, the confidence-threshold learner is fragile and under-generalized encountering domain knowledge shift. Moreover, at the most time, the target domain is agnostic in training. Hence, it is imperative to exploit how to enhance the generalization of confidence-threshold locator to the latent target domain. In this paper, we propose a Dynamic Proxy Domain (DPD) method to generalize the learner under domain shift. Concretely, based on the theoretical analysis to the generalization error risk upper bound on the latent target domain to a binary classifier, we propose to introduce a generated proxy domain to facilitate generalization. Then, based on the theory, we design a DPD algorithm which is composed by a training paradigm and proxy domain generator to enhance the domain generalization of the confidence-threshold learner. Besides, we conduct our method on five kinds of domain shift scenarios, demonstrating the effectiveness on generalizing the crowd localization. Our code will be available at <https://github.com/zhangda1018/DPD>.

**Index Terms**—Dynamic Proxy Domain, Crowd Localization, Domain Adaptation, Binary Segmentation.

## I. INTRODUCTION

CROWD localization aims to predict each instance precise location within the image. Since the task owns wide latent applications, it attracts many researchers' attention, which makes the fully supervised crowd localization achieved great success [1], [2], [3], as a result of some advanced pipelines [4], [5] and training paradigms [6], [7]. Nevertheless, the great performance is built on the ocean of annotated data, and the mainly adopted *Empirical Risk Minimization* (ERM) gives an assumption of testing data being with the independent identically distributed to annotated ones. It is obvious that the assumption is vulnerable under the data sampled from real crowd scenes, and when it is violated, the superior performance would be collapsed. What's more, how the crowd scenes exhibits to the trained crowd locator will be blind in testing, which means the target domain distribution is agnostic to us during training. To this end, how to improve the generalization to the latent target domain of

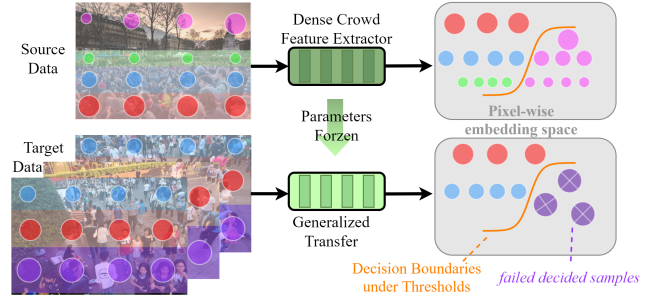


Fig. 1. The superior performance achieved by existing segmentation based crowd locators mostly depends on the robust threshold to classify the samples into two parts. However, when transferring the threshold to another domain, the specific knowledge incurs some samples are ineffective under the thresholds.

crowd locator trained on a source domain is significant. Hence, this paper targets on stabilizing crowd localization performance or generalizing it when encountering data distribution not obeying, namely target agnostic domain generalization.

To begin with, we make analysis on the specific points for crowd localization under domain shift issue. As aforementioned, the advanced pipelines create superior performance on crowd localization. Such as [8], [9] proposed to treat crowd localization as a binary segmentation task, in which the heads area are segmented into foregrounds. However, due to the variance to the semantic knowledge to pedestrians (like instance scale, exhibition or scene style), the crowd locator has different confidence to instances within an image. Therefore, [10] proposes a novel adaptive pixel-wise threshold learner to realize variance aware pixel-wise binary classification according to the extracted features. Then, fully supervised training paradigm minimizes the empirical risk on training set (or source domain), which means the threshold learner is targeting on reducing the empirical loss along with non-convex loss landscape on annotated data in the source domain.

Unfortunately, crowd scenes are inherently prone to significant variations across images or datasets due to uncertainties in crowd features, such as scene layout, crowd count, and camera perspective, among others. This leads to challenges in handling unseen scenes, commonly known as the domain shift issue. In such cases, the crowd locator often exhibits low confidence in object localization while expressing excessive confidence in background regions. An illustrative example is presented in Fig. 1. Additionally, misembedded features can lead to irrational adaptive thresholds. Consequently, when the empirical risk minimization process in the source domain

Junyu Gao and Da Zhang are with the School of Artificial Intelligence, Optics and ElectroNics (iOPEN), Northwestern Polytechnical University, Xi'an 710072, China and with the Key Laboratory of Intelligent Interaction and Applications, Ministry of Industry and Information Technology, Xi'an 710072, P. R. China. (E-mail: gjy3035@gmail.com; dazhang@mail.nwpu.edu.cn). Xuelong Li is with the Institute of Artificial Intelligence (TeleAI), China Telecom Corp Ltd, 31 Jinrong Street, Beijing 100033, P. R. China. (E-mail: xuelong\_li@ieee.org)

rigidly steers the confidence threshold learner towards the fixed source distribution, any domain shift exacerbates the difficulty of achieving effective generalization to the target domain. Paradoxically, pushing the model to overfit on the source distribution through ERM intensifies the source knowledge while distancing target specific knowledge, a phenomenon known as the *Matthew Effect*. To this end, how to better balance confidence with threshold is the key to realize crowd localization under domain generalization.

Based on the above observation, we propose a domain generalization framework for crowd localization, **Dynamic Proxy Domain (DPD)**, which is an attempt based on the analysis to the upper bound of the generalization error on target domain. To be specific, we treat the confidence-threshold learner as a 0-1 classifier. Then, theoretically analyzing the generalization error upper bound on target domain, we propose to generalize the source domain trained model via introducing a new dynamic domain as the proxy one. Furthermore, the ERM is able to push the model towards the dynamic domain distribution, but not the fixed source one, which make it feasible to improve the generalization on target domain. According to the exploited theoretical guarantees, we design the corresponding algorithm, which is composed by the usage of source sample, proxy domain generator and a convergence strategy. In summary, the contributions of our work can be three-fold:

- Propose to tackle the domain generalization of crowd localization from the perspective of generalizing the confidence-threshold learner. To the best of our knowledge, this paper is the first attempt on the issue.
- Present that a dynamic proxy domain generated from source only data improves the generalization for binary segmentation based crowd locator and provide rigorous theoretical guarantees.
- Based on the theory, we design an algorithm of introducing dynamic proxy domain and its corresponding training paradigm. Conduct experiments to provide empirical guarantees.

## II. RELATED WORK

In this section, we array some related work to our DPD, which can be divided into two parts.

### A. Crowd Analysis

The existing crowd analysis can be counting and localization (detection). Crowd counting has achieved superb development, due to its succinct but effective framework [11], [4]. Moreover, some studies extend it into more fields, such as multi-modal [12], multi-view [13], un-/semi-/weakly/noisy [11], [14], [15], [16] supervised learning. Then, the crowd localization also attracts some research attention because it provides more information than counting since. The purpose of crowd localization is to locate the exact position of each head in a scenario. The earlier locators are firstly based on object detection [17], [18]. TinyFaces [19] uses a detection-based framework to locate tiny faces by analyzing the effects of scale, contextual semantic information, and image resolution. Following this

some researchers have done extended work in addressing intrinsic scale shifts [20], [21] but detection-based methods still perform poorly in extremely congested situations. Besides, some points-based locator [22], [23], [24] are proposed. Li et al. [24] proposed a multi-focus gaussian neighborhood attention to estimate exact locations of human heads in the given crowded videos. Although these methods worked to some extent but they can't provide scale information and performance is still undesirable. Thus, the pixel-wise binary segmentation [8], [10] is proposed for crowd localization. However, the training of thresholds suffer from overfitting on training data (source domain). To generalize it to the target agnostic domains, we propose DPD.

### B. Cross Domain Convergence

The existing machine learning methods depend on training with a multitude of data. To this end, the data distribution shift namely domain shift between training with testing impedes the generalization of the models. Hence, Wen et al. [25] first propose to enhance the performance on target domain via introducing some unlabeled target data, namely *Domain Adaptation (DA)*. Subsequently, some DA methods have been proposed [26], [27]. In DA, the traditional paradigms include adversarial training [28], self-training [29] and few shot learning [30]. Several methods attempt to adapt domains through finding their similarities [31], [32] while other try to find common knowledge between them [33], [34]. However, at most time, the target domain is totally agnostic to us in training, which is the task of *Domain Generalization (DG)*. Since there are only training samples and we do not know how the target domain distributed, the goal mainly focuses on enhancing the generalization and reducing overfitting to source domain. In this paper, our DPD achieves the two purposes via converging on source domain and dynamic proxy domain simultaneously.

## III. PRELIMINARIES

### A. Supervised Crowd Localization

In crowd localization [8], given a crowd image represented by  $x \in \mathbb{R}^{3 \times H \times W}$ , the encoder  $h_E$  in locator maps the image to a latent feature  $h_E(x)$ , which has a greater channel but lower resolution than the original image. The decoder  $h_D$  utilizes this latent feature to generate a confidence map  $y_{prec}^c \in \mathbb{R}^{1 \times H \times W}$ , where the confidence values indicate the likelihood of a given pixel being in pedestrians' head area. Then, a fixed threshold of 0.5 (due to binary segmentation) classifies the confidence into two parts and generates a binary map in Fig. 2. Ideally, the relationship between  $y_{prec}^c$  and ground truth binary map of  $y_{gt}^b$  should be formulated as shown in Eq. 1:

$$\begin{cases} \lim_{y_{gt}^b(i,j)=1} y_{prec}^c(i,j) \rightarrow 1^- & , (i,j) \in (H,W); \\ \lim_{y_{gt}^b(i,j)=0} y_{prec}^c(i,j) \rightarrow 0^+ & , (i,j) \in (H,W), \end{cases} \quad (1)$$

in which a fixed threshold could separate confidences belonging to fore-/backgrounds well. However, the instances among the crowds could be with huge variance and make predicted

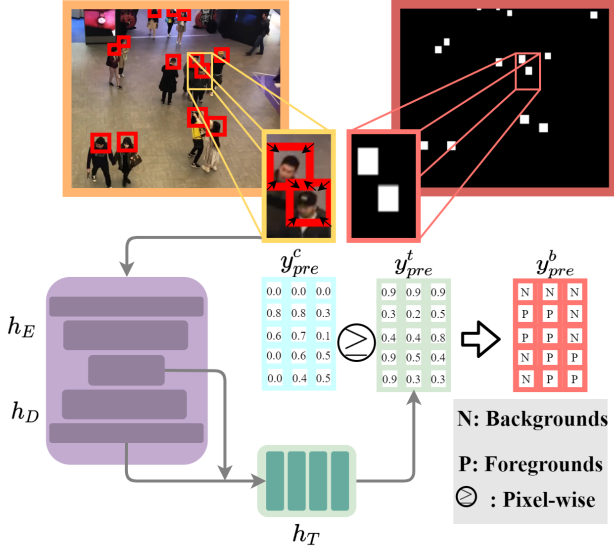


Fig. 2. A toy example for the pipeline of adaptive instance crowd localization. To facilitate visualization, only the image patch in yellow window are fed into crowd locator.

confidence value in  $y_{prec}^c$  very low on some hard/rare samples. For instance, the decoder  $h_D$  struggles to always regress  $y_{prec}^c(i, j)$  towards 1 in head area and 0 in backgrounds, making it difficult to achieve accurate predictions. As a result, a fixed threshold fails to detect such instances.

To overcome this limitation and obtain precise predictions, Gao et al. [10] introduces a pixel-wise threshold map to adaptively separate  $y_{prec}^c$  into a binary map  $y_{prec}^b$ . Hence, the learner namely locator is fed with an image  $x \in \mathbb{R}^{3 \times H \times W}$  along with its corresponding binary map annotation  $y \in N_{\{0,1\}}^{1 \times H \times W}$ , composing  $(x_i, y_i)_i^n$  sampled from a data distribution space  $\mathcal{X} \times \mathcal{Y}$ . In order to derive an adaptive threshold map based on the latent feature  $h_E(x)$ , the threshold learner  $h_T$  is proposed to map  $h_E(x)$  and  $y_{prec}^c$  into a threshold map  $y_{prec}^t \in \mathbb{R}^{1 \times H \times W}$ . The learned threshold map  $y_{prec}^t$  enables it to lower the threshold for hard instances that are predicted with lower confidence by  $h_D$ . This aids to produce a more robust binary map which can be estimated via Eq. 2:

$$y_{prec}^b = \lceil y_{prec}^c \geq y_{prec}^t \rceil, \quad (2)$$

where  $y_{prec}^c \in \mathbb{R}^{1, H, W}$  is from Eq. 3,

$$\begin{aligned} y_{prec}^t &= h_T[h_E(x) * y_{prec}^c], \text{ in which} \\ y_{prec}^c &= \text{Sigmoid}\{h_D[h_E(x)]\}, \end{aligned} \quad (3)$$

and the  $\lceil \cdot \rceil$  is the pixel-wise Iverson bracket. A visual representation of the process can be found in Fig. 2. To this end, according to the above arrayed process and the mapping function  $h$  in the annotation space  $\mathcal{H}$  can be induced as Eq. 4, which means to find the best pixel-wise classification prediction  $y_{pred}^b$  such that the difference from the actual pixel classifications  $y$  is minimized:

$$h : x \mapsto \arg \max_{y_{pred}^b \in \mathcal{X} \times \mathcal{Y}} \sum_i^{H \times W} y_{pred}^b \oplus y. \quad (4)$$

However, [10] further enhances the training via adding an optimization term to  $y_{prec}^c$ . The empirical risk of a given  $h \in \mathcal{H}$  are formulated as Eq. 5,

$$\widehat{R}_{\mathcal{X} \times \mathcal{Y}}(h) \triangleq \frac{1}{N} \sum_{i=1}^N [\mathcal{L}_2(y_{prec}^c, y) + \mathcal{L}_1(y_{prec}^b, y)], \quad (5)$$

in which the  $\mathcal{L}_n(\cdot, \cdot)$  represents the norm  $n$  loss function. Hence, the Empirical Risk Minimization (ERM) function is:

$$ERM_N = \arg \min_{h \in \mathcal{H}} \widehat{R}_{\mathcal{X} \times \mathcal{Y}}(h). \quad (6)$$

To better clarify the pipeline of adaptive threshold crowd localization, a pseudo code is arrayed in the Appendix A-A. However, when the testing data does not obey *i.i.d.* (namely domain generalization issue) after training with Eq. 6, the distribution of  $\Pr(y_{prec}^c)$  and  $\Pr(y_{prec}^t)$  tend to be irrational, *i.e.* as shown in Eq. 7.

$$\begin{cases} y_{prec}^c \geq y_{prec}^t, & y = 0 \\ y_{prec}^c < y_{prec}^t, & y = 1 \end{cases} \quad (7)$$

Based on the issue, we will provide some theoretical preliminaries on the irrationality under domain generalization.

### B. Theoretical Analysis on Cross Domain Convergence

Let  $\mathcal{D}_s$  be the set of source domain, which is a distribution involving input crowd sample space  $\mathcal{X}_s$  along with its ground truth annotations space  $\mathcal{Y}_s$ . Then, another domain  $\mathcal{D}_t$  is introduced as the target distribution, which is defined as  $\mathcal{X}_t \times \mathcal{Y}_t$ . In practice, the domain generalization task is fed with a source sample  $\mathcal{S}$  drawn *i.i.d.* among  $\mathcal{D}_s$ , as the Eq. 8 shown,

$$\mathcal{S} = \{(x_i^s, y_i^s)\}_{i=1}^{n_s} \sim \mathcal{D}_s. \quad (8)$$

Next, let  $h$  be the mapping function of binary classifier, the error risk on target space  $\mathcal{D}_t$  is as Eq. 9:

$$R_{\mathcal{X}_t \times \mathcal{Y}_t} \triangleq \Pr_{(x_t, y_t) \sim \mathcal{D}_t} \{ \vec{\delta} [h(x_t) \neq y_t] \}, \quad (9)$$

where  $\vec{\delta}$  is the two dimensional Dirac function.

In domain generalization, the pain point is that the optimization objective is on target samples, while the real training is done on source samples. To this end, the discrepancy between distributions incurs model with low error risk on source domain hard to be also generalized well on target domain. That is, it's difficult to balance the discrepancy between Eq. 6 and minimizing Eq. 9. More specifically, the discrepancy between distributions is the key. Hence, the former researchers [35] leveraged  $\mathcal{H} \Delta \mathcal{H}$ -divergence to measure the discrepancy:

**Definition 1.** Let  $\mathcal{D}_s$  and  $\mathcal{D}_t$  be the two aforementioned domains distribution,  $h$  is the hypothesis to the labeled function, while  $h_s$  is the converged one. The  $\mathcal{H} \Delta \mathcal{H}$ -divergence between  $\mathcal{S}$  with  $\mathcal{T}$  is

$$\text{div}_{\mathcal{H} \Delta \mathcal{H}} = \sup_{h_s, h \in \mathcal{H}} |\mathbb{E}_{\mathcal{S}}[h_s \neq h] - \mathbb{E}_{\mathcal{T}}[h_s \neq h]|_1. \quad (10)$$

However, given a sampled data set from distribution, the Def. 1 is limited and hard to be computed. Thus, [35] approximate it by introducing Def. 2 via a proxy divergence:

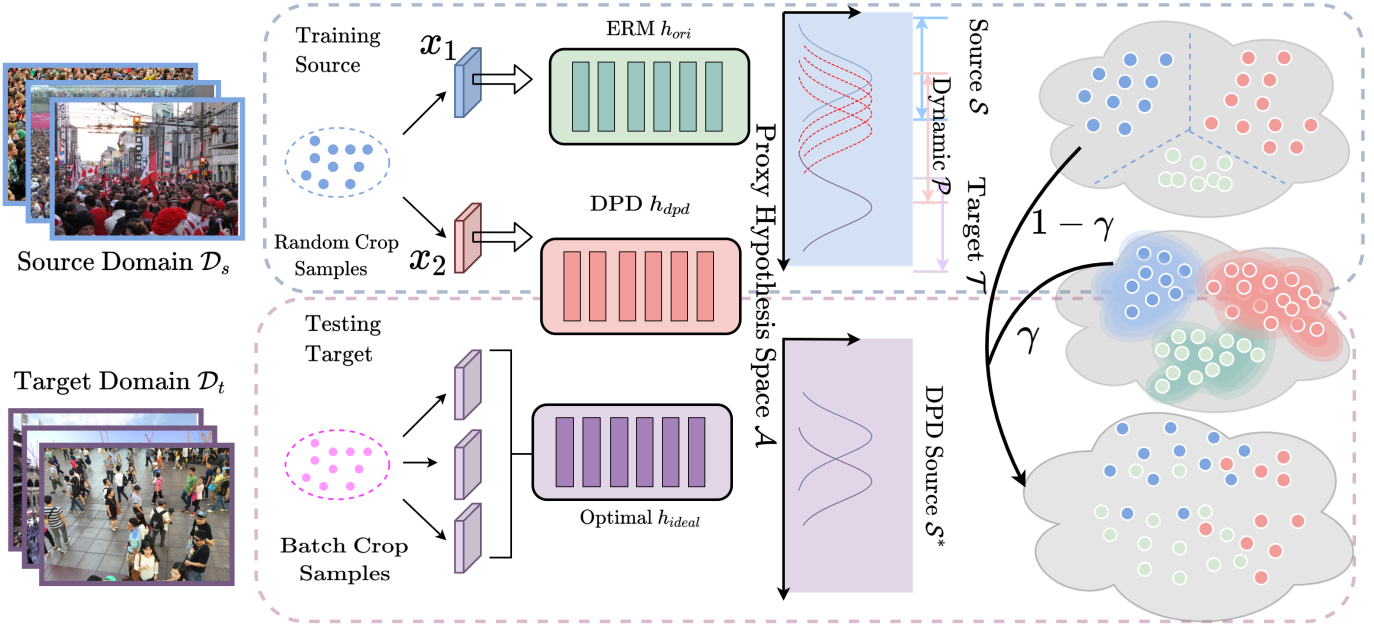


Fig. 3. Overview of our core idea to the proposed **Dynamic Proxy Domain**. Comparing with implementing ERM on the source domain, we introduce DPD which minimizes the divergence between source distribution with target distribution. To this end, the decision boundary among domains can be weakened on the hypothesis space  $\mathcal{A}$ .

**Definition 2.** A proxy dataset is constructed as:

$$\mathcal{X}_{prox} = \{(x_i, [x_i \sim \mathcal{D}_s]) | i \in \{0, \dots, N_s + N_t\}\}. \quad (11)$$

A proxy generalized error  $\epsilon_p$  is introduced on  $\mathcal{X}_{prox}$ . Then, the  $\mathcal{H} \Delta \mathcal{H}$ -divergence can be approximated as:

$$\hat{d}_{\mathcal{A}} = 2 \cdot (1 - 2\epsilon_p) = 2 \sup_{A \in \mathcal{A}} |Pr_{\mathcal{D}_s}(A) - Pr_{\mathcal{D}_t}(A)|. \quad (12)$$

Given the discrepancy between two domains, we are ready to measure the empirical risk on target domain under the cross domain settings. More specifically, the upper bound on the target error risk can be formulated as Lemma 1, which is proposed and expanded in [36]:

**Lemma 1.** Assume that the  $\mathcal{H}$  is a hypothesis space with a VC dimension of  $d$  and  $m$  is the number of training samples, drawn from  $\mathcal{D}_s$ . Given an  $h \in \mathcal{H}$ , which is a binary classifier, the following inequality holds (specific proof is in Appendix B.) with a probability at least  $1 - \delta$ , where  $\delta \in (0, 1)$ :

$$R_{\mathcal{T}}(h) \leq \hat{R}_{\mathcal{S}}(h) + \frac{1}{2} \hat{d}_{\mathcal{H} \Delta \mathcal{H}}(\mathcal{S}, \mathcal{T}) + 4 \sqrt{\frac{2d \log(2m) + \log(\frac{2}{\delta})}{m}} + \lambda, \quad (13)$$

in which

$$\lambda = \inf_{\hat{h} \in \mathcal{H}} [R_{\mathcal{S}}(\hat{h}) + R_{\mathcal{T}}(\hat{h})]. \quad (14)$$

In Lemma 1, the first term namely  $\hat{R}_{\mathcal{S}}(h)$  is empirical error risk on source domain, which can be very low as our training paradigm is based on ERM. As for the last term namely  $\lambda$ , when the  $\lambda$  is large, it is impossible to generalize model to the  $\mathcal{D}_t$ . Finally, our optimization target lies on the two terms in the middle of Eq. 13.

## IV. METHODOLOGY

### A. Theory of Dynamic Proxy Domain

To begin with, we notice in the third term of Eq. 13, the hypothesis space  $\mathcal{H}$  is defined on a VC-dimension of  $d$ , which is fixed, and  $\delta$  is the probability, which cannot be optimized. To this end, let us concentrate on the  $m$  which is the number of source samples.

**Theorem 1.** Let  $h^*$  be the optimal hypothesis of  $h$  and  $m^*$  is the corresponding number of samples, which are all defined on  $\mathcal{H}$  with a VC-dimension of  $d$ , i.e.,  $h^* = \arg \min_{h \in \mathcal{H}} R_{\mathcal{T}}(h)$ . Then, for any  $\delta \in (0, 1)$ , with probability at least  $1 - \delta$ , we have:

$$R_{\mathcal{T}}(h) - \inf_{h \in \mathcal{H}} R_{\mathcal{T}}(h^*) \leq \hat{R}_{\mathcal{S}}(h) - \inf_{h \in \mathcal{H}} \hat{R}_{\mathcal{S}}(h^*) + \sup_{m^* \in [1, +\infty)} \sqrt{\frac{2d \log(2m^*) + \log(\frac{2}{\delta})}{m^*}} + \sqrt{\frac{2d \log(2m^*) + \log(\frac{2}{\delta})}{m^*}}, \quad (15)$$

let  $\Delta R_{\mathcal{T}}(h; h^*)$  be the left hand item, then we have Eq. 16 holds.

$$m^* = \arg \min_{h, h^* \in \mathcal{H}} \Delta R_{\mathcal{T}}(h, h^*; m) = \sup_{m \in \mathbb{R}} m. \quad (16)$$

**Proof.** To begin with, let  $\varepsilon(m) = \sqrt{\frac{2d \log(2m) + \frac{2}{\delta}}{m}}$ . Obviously, when the  $m$  is given, the  $\varepsilon(m)$  is also a constant, which means its supremum over the variant  $m$  is fixed. To this end, we put our concentration on the analysis to the monotonicity of  $\varepsilon(m)$ .



Then, we firstly omit the radical, since it incurs nothing on the monotonicity to  $\varepsilon(m)$ . Thus, we have:

$$\frac{\partial \varepsilon}{\partial m} = \frac{\frac{1}{m} \cdot m - [2d \cdot \log(2m) + \log(\frac{2}{\delta})]}{m^2} < 0, \text{ if and only if: } m \in [1, +\infty). \quad (17)$$

The Thm. 1 indicates the optimization gap from the updated hypothesis  $h$  to the optimal hypothesis  $h^*$ . Thus, we hope that the  $\Delta R_{\mathcal{T}}(h; h^*)$  should be deduced while training. To this end, we find that the error gap is related to the number of samples. According to Eq. 16, the error gap has a relevance of negative. Hence, to deduce error gap, the number of samples fed into optimization should be more.

After analyzing the third term in Eq. 13, let us put concentration on the second term, namely the  $\mathcal{H} \Delta \mathcal{H}$ -divergence between source and target domains. Theoretically, the Def. 1 tells us once the source domain  $\mathcal{S}$  and target domain  $\mathcal{T}$  are given, the  $\mathcal{H} \Delta \mathcal{H}$ -divergence is fixed. Hence, minimizing *empirical risk* on the fixed source domain  $\mathcal{S}$  cannot generalize well on target domain  $\mathcal{T}$ . Furthermore, despite that in the crowd scenes samples, there is no clear boundary between  $\mathcal{S}$  with  $\mathcal{T}$ . In other word, we cannot say the  $\mathcal{D}_s$  is strictly independent with  $\mathcal{D}_t$  in the hypothesis space  $\mathcal{H}$ . But converging on  $\mathcal{D}_s$  incurs the performance on  $\mathcal{D}_s$  specific knowledge is zoomed, while on the invariant knowledge is worse.

Based on the above analysis, directly minimizing the *empirical risk* on the fixed  $\mathcal{D}_s$  is useless in reducing the  $\mathcal{H} \Delta \mathcal{H}$ -divergence. To this end, we propose to introduce a *dynamic proxy domain*  $\mathcal{P}$  to facilitate the obstinate source domain being more flexible in reducing  $\mathcal{H} \Delta \mathcal{H}$ -divergence. Considering the empirical risk on source or our DPD is optimized via ERM, the only gap lies on divergence term and the term with  $m$ . So we have proven enhancing  $m$  introduces generalization. Then, we will prove that how the DPD influences the divergence.

**Corollary 1.** Let  $h^*$  be the worst case of  $h$  in  $\mathcal{H}$ , for  $\delta \in (0, 1)$ , w.p.b. at least  $1 - \delta$ , for all  $h^* \in \mathcal{H}$ ,

$$R_{\mathcal{T}}(h^*) \leq \max_{\gamma \in [0, 1]} \Theta(h^*), \quad (18)$$

where  $\Theta$  is the right hand term in Eq. 13. Then, when Eq. 18 holds, we have  $\gamma = 1$ .

Once the Coro. 1 holds, namely  $h = h^*$ , the Eq. 13 holds. It is obvious that as long as DPD is introduced, the  $\gamma \leq 1$ , or the process is meaningless. By now, we demonstrate introducing a new domain is helpful in enhancing generalization.

## B. Algorithm

According to the above theoretical guarantees, we design the corresponding algorithm. To begin with, in Lemma. 1, it tells that the generalization error risk on target domain  $R_{\mathcal{T}}$  can be bounded from two terms, which are  $\varepsilon(m)$  and  $div_{\mathcal{H} \Delta \mathcal{H}}(D_{\mathcal{S}}, D_{\mathcal{T}})$ . Moreover, we still need to consider the empirical risk. All in all, our objective function firstly can be:

$$\min_{h \in \mathcal{H}} [\hat{R}_{\mathcal{S}}(h) + \varepsilon(m) + div_{\mathcal{H} \Delta \mathcal{H}}^{h, \mathcal{H}}(D_{\mathcal{S}}, D_{\mathcal{T}})]. \quad (19)$$

1) *Momentum Network for Usage of Source Data*: Recall that Eq. 19 shows the three terms of our objective. In this subsection, we show how the DPD optimizes the first two terms. For the  $\hat{R}_{\mathcal{S}}(h)$ , it is a normal ERM process. Thus, given a batch of samples  $\mathbf{x} \in \mathbb{R}^{B \times 3 \times H \times W}$ , the hypothesis  $h$  is able to map it into  $\mathbf{y}_{pre}^c \in \mathbb{R}^{B \times 1 \times H \times W}$  and  $\mathbf{y}_{pre}^b \in \mathbb{N}_{\{0, 1\}}^{B \times 1 \times H \times W}$ . For the ERM part, the optimization problem can be arrayed:

$$\min_{h \in \mathcal{H}} (\|\mathbf{y}_{pre}^c - \mathbf{y}\|^2 + \|\mathbf{y}_{pre}^b - \mathbf{y}\|^1). \quad (20)$$

The Thm. 1 tells that a larger  $m$  can effectively reduce  $\varepsilon(m)$ . However, due to batch manner training, we cannot introduce too many samples in one gradient descend (GD) step. To this end, we propose a *Momentum Updated Model*  $h_{Mo}$  to equally achieve zooming  $m$ . Moreover, thanks to the usually adopted training paradigm in crowd localization, namely *random crop*, we can fully utilize it to further enhance the zooming.

To be concrete, given two cropped source images, which are  $\mathbf{x}_1, \mathbf{x}_2 \in \mathbb{R}^{B \times 3 \times H \times W}$ , we utilize one of them namely  $\mathbf{x}_1$  to train with ERM through Eq. 20. Then, another crop  $\mathbf{x}_2$  is predicted by  $h$  and  $h_{Mo}$  simultaneously. Finally, a consistency constraint is introduced:

$$\min_{h, h_{Mo} \in \mathcal{H}} (\|\mathbf{y}_{pre}^c - \mathbf{y}_{Mo}^c\|^2 + \|\mathbf{y}_{pre}^b - \mathbf{y}_{Mo}^b\|). \quad (21)$$

In addition, the parameters of momentum model  $\theta_{Mo}$  are updated as:

$$\theta_{Mo} \leftarrow \mu \cdot \theta_{Mo} + (1 - \mu) \cdot \theta_h, \quad (22)$$

where  $\mu \in [0, 1]$  is the updating coefficient. Through combining Eq. 21 with Eq. 20, the ERM reduces the  $\hat{R}_{\mathcal{S}}(h)$  on the one hand, and the number of training samples  $m$  is zoomed on the other hand.

2) *Dynamic Proxy Domain*: In this subsection, we will show how our proposed *Dynamic Proxy Domain* is introduced. To begin with, we refer to the theoretical guarantees, in which a *dynamic proxy domain* facilitates the generalization. Therefore, the key lies on the generation of the dynamic proxy domain  $\mathcal{D}_p$ . Firstly, the Lemma. 1 tells us as the fitting degree being enhanced, the generalization is weaker as a result of the existence of  $\hat{d}_{\mathcal{H} \Delta \mathcal{H}}(\mathcal{S}, \mathcal{T})$ . However, since the source domain is all knowledge we have, there seems no other way to let crowd locator get the localization knowledge (how to embed the image into instance confidence and threshold). To this end, we notice that the parameters before overfitting on source domain could reserve more generalized knowledge (but less localization knowledge). Inspired by this, we propose that the generation of  $\mathcal{D}_p$  could be based on the model prediction before overfitting. A toy example has been illustrated as Fig. 4. By now, we notice that the Eq. 21 also minimizes the risk on generated history domain via Momentum model, which is composed of history parameters. However, the Eq. 22 suggests that the parameters of Momentum model is being pushed to the main model, which can be deemed as overfitted one. Thus, we propose to generate  $\mathcal{D}_p$  in the second order.

To be specific, we propose a *Dynamic  $\mathcal{H} \Delta \mathcal{H}$ -generator* namely  $h_T^{\mathcal{H} \Delta \mathcal{H}}$ , which is an independent threshold learner and also defined on the same  $\mathcal{H}$  space. Concretely, the *Dynamic Proxy Domain* is generated via  $h_T^{\mathcal{H} \Delta \mathcal{H}}$ . Moreover, the  $h_T^{\mathcal{H} \Delta \mathcal{H}}$

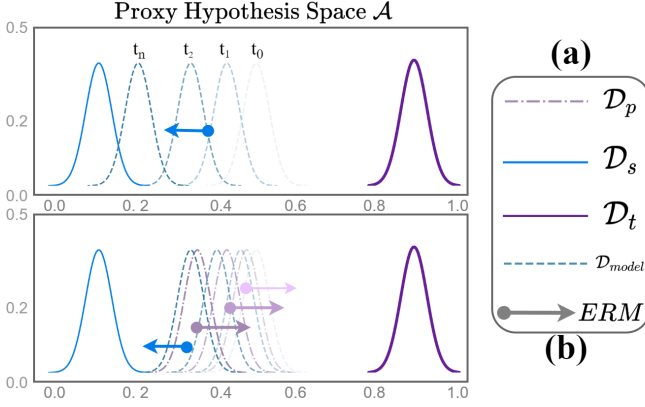


Fig. 4. (a) Convergence to the fixed source domain. (b) Convergence to the source domain along with dynamic proxy domain simultaneously.

has the independent optimizer to update. Then, we can concatenate the proposed  $h_T^{\mathcal{H}\Delta\mathcal{H}}$  into the Momentum model in Sec. IV-B1.

To begin with, we pick one crop between  $\{x_1, x_2\}$ . Then, the corresponding  $y_{pre}^c$  is fed into the original threshold learner  $h_T^{ori}$  along with  $h_T^{\mathcal{H}\Delta\mathcal{H}}$  simultaneously. By now, the  $h_T^{\mathcal{H}\Delta\mathcal{H}}$  is able to generate  $\mathcal{D}_p$  predictions during dynamic training. Then, to reduce the  $d_{\mathcal{H}\Delta\mathcal{H}}(\mathcal{D}_p, \mathcal{D}_s)$ , our objective can be:

$$\min_{h, h_T^{\mathcal{H}\Delta\mathcal{H}} \in \mathcal{H}} (\mathcal{L}[h(x_s), h_T^{\mathcal{H}\Delta\mathcal{H}}(x_s)]), \quad (23)$$

where  $\mathcal{L}(\cdot, \cdot)$  denotes the loss function.

To better utilize the introduced DPD, we exploit a training strategy that in the convergence of Eq. 23, a *stronger* loss should be implemented than the one utilized in the second term of Eq. 20. In this paper, we adopt a combined loss of:

$$\mathcal{L}_T^{\mathcal{H}\Delta\mathcal{H}} = 1 - \frac{2 \cdot \|y_{pre}^b \circ y_{dpd}^b\|_1}{\|y_{pre}^b\|_1 + \|y_{dpd}^b\|_1} + \|y_{dpd}^b - y_{pre}^b\|_1. \quad (24)$$

Finally, our objective is summing up the Eq. 20, Eq. 21 and Eq. 23. We provide pseudo code of Dynamic Proxy Domain Algorithm in Appendix A-B.

TABLE I  
THE *Monte Carlo Uncertainty* VALUES ARE ARRAYED WHEN THE DATASETS ARE ADOPTED AS THE TARGET DOMAINS. THE BOLD VALUES REPRESENT BETTER RESULTS.

Datasets	Monte Carlo Uncertainty <sup>↓</sup>				
	JHU	SHHB	FDST	QNRF	NWPU
Adaptive	0.359	0.358	0.351	0.359	0.357
DPD	<b>0.123</b>	<b>0.069</b>	<b>0.062</b>	<b>0.238</b>	<b>0.113</b>

## V. EXPERIMENTS

### A. Datasets

In this paper, we conduct our DPD on six datasets, which are SHHA [37], SHHB [37], QNRF [38], JHU [39], NWPU [40] and FDST [41].

- **ShanghaiTech PartA(SHHA)** [37], which is composed by 270 training images, 30 validation images and 182 testing images.

- **ShanghaiTech PartB(SHHB)** [37], which is composed by 360 training images, 40 validation images and 316 testing images.
- **UCF-QNRF(QNRF)** [38], which is composed by 961 training images, 240 validation images and 334 testing images.
- **JHU-Crowd++(JHU)** [39], which is composed by 2,772 training images, 500 validation images and 1,600 testing images.
- **NWPU-Crowd(NWPU)** [40], which is composed 3,109 training samples, 500 validation samples and 1500 testing samples.
- **FudanShanghaiTech(FDST)** [41], which is composed by 150,000 frames from 13 different scenes, where 7,800 frames are for training, 1,200 frames are for validation and 6,000 frames are for testing.

To further show the main statistic information and the domain shift existing among them, we array some main features of the datasets in Appendix C. To begin with, we pick some explicit domain specific knowledge to array. For the RGB images, the pixel values distribution is one of the domain specific knowledge, due to the RGB distribution representing the scene style. As the Appendix Fig. 12 shown, SHHA owns clear distribution with other datasets. Then, for crowd scenes, the resolution level, congested level and scale level also make great influence to the convergence. Hence, we show that despite that the counting of SHHA is not least, considering its average resolution, the quality of SHHA is worst. Finally, we calculate the annotated boxes area as the scale information to the instances and present the scale shift to datasets as shown in Appendix Fig. 12. To this end, we pick the **weakest** dataset, which means least information, SHHA as our source domain, while other datasets are adopted as target domain.

### B. Implementation Details

In the training phase, the training data only comes from SHHA[37] and the model is tested on the target sets. For code backgrounds, we leverage a PyTorch framework of C3F[42] on an NVIDIA A100 GPU with a memory of 80Gb. For data preparing, we randomly crop the original images with a resolution of  $(512 \times 512)$ , then an augmentation of random rescale with a range of  $[0.8, 1.2]$  and a probability of 0.5 for horizontal flip are leveraged. For network, a backbone model of VGG-16 [43] and Feature Pyramid Network(FPN) [44] are adopted. For training, a batch size of 8, an optimization of Adam [45] along with a learning rate of  $1e-5$  are utilized. To measure the performance on crowd localization, we utilize F1-measure (F1-m), precision(Pre.) and recall(Rec.), in which the F1-m is the primary metric.

$$\begin{aligned} \text{Pre.} &= \frac{TP}{TP + FP}, \\ \text{Rec.} &= \frac{TP}{TP + FN}, \\ \text{F1-m} &= \frac{2 \cdot \text{Pre.} \cdot \text{Rec.}}{\text{Pre.} + \text{Rec.}}. \end{aligned} \quad (25)$$

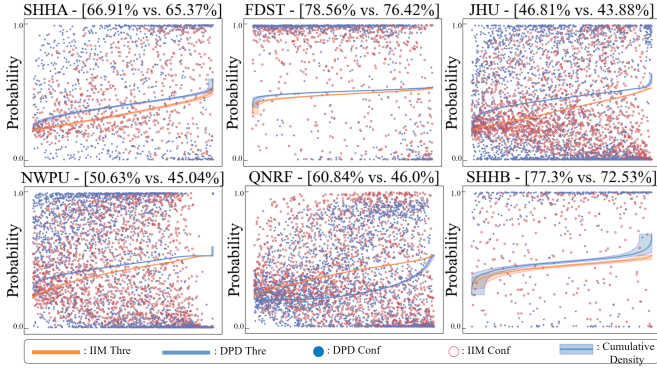


Fig. 5. The confidence and threshold distribution on six adopted datasets with IIM along proposed DPD. The scatters in the figure are the confidences, while the plots are the thresholds, in which the shadow area denotes the density of the values, the bigger of the shadow areas, the lower of the density is. The compared ratio is the confidence larger than its threshold.

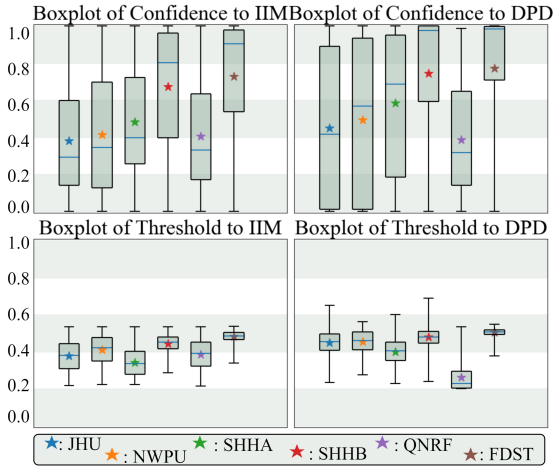


Fig. 6. The boxplot of confidences (upper row) / thresholds (lower row) distribution between the IIM [10] with DPD, in which the line in the box denotes the median and the star denotes the mean value to the distribution.

### C. Discussion on Our Method

1) *Comparison between DPD with IIM*: In this part, we visualize the confidence and threshold distribution of the positive pixels. To be concrete, our motivation is from the irrational distribution between confidence and threshold. The irrationality comes from two perspectives. 1) The threshold is not generalized and only limited within a small value band (see Fig. 5 & 6). 2) The uncertainty of confidence is large, which is incurred by under-fitting to target domain (see Table. I).

Then, we make further accurate and fastidious analysis. As shown in Fig. 6, we array the boxplot of the confidences and thresholds distributions on six target domains (including SHHA-test). To be concrete, the upper and lower quartile, median and extremum values are exhibited. According to the Fig. 6, we notice some general phenomenon. 1) The range of thresholds in DPD is expanded comparing with IIM; 2) The compactness of the DPD distribution is enhanced; 3) The average thresholds are improved except for QNRF. Then, we make discussion on the three aforementioned phenomenon.

For 1), a wider range of thresholds are obtained by introducing DPD. It is obvious that our DPD endows the

threshold learner more tolerance to the outliers. As for 2), the convergence to the non-convex loss landscape is inclined to overfit on the normal samples. However, the thresholds arrayed in Fig. 6 are all measured as target domain, which means the introduction of DPD indeed enhances the generalization. Considering 3), the QNRF dataset is extremely congested, which means it is more obscure than the source domain. Also, as the Fig. 5 and 6 shown, the average confidences on the QNRF is the lowest comparing with other datasets. Hence, to adapt to the difficulty of QNRF, our DPD pushes the thresholds towards 0. Then, for other datasets, the improvement can be similar. We also provide visualization results in Appendix Fig. 13 for both methods.

Besides, to measure how the uncertainty changes after introducing DPD, we compute them directly. The computation process is based on the *Monte Carlo Uncertainty*:

$$U_{MCU} = -\frac{1}{N} \sum_{i=1}^N \text{conf}_i \cdot \log(\text{conf}_i), \quad (26)$$

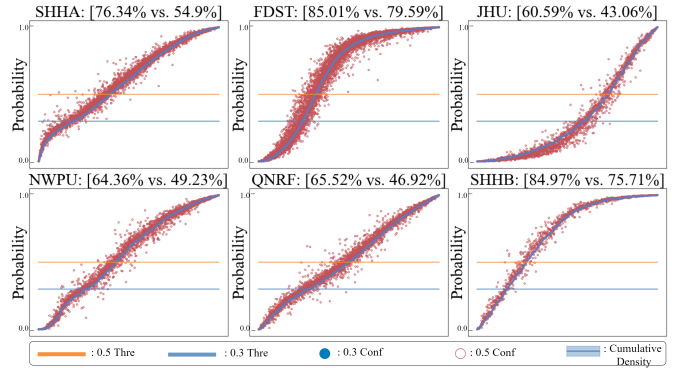


Fig. 7. The confidence distribution to the crowd locator trained with the fixed thresholds, namely 0.3 and 0.5.

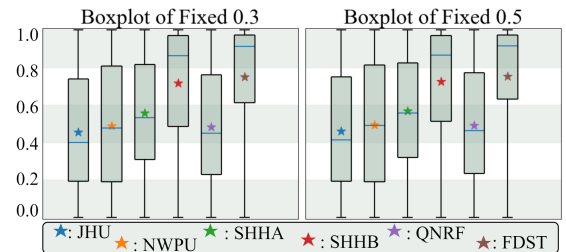


Fig. 8. The boxplots of six adopted datasets, in which the left one is from IIM results, while the right one is from our proposed DPD results. The upper row is confidence, while lower row is threshold.

2) *Comparison between Fixed 0.3 with 0.5*: In this subsection, we compare the crowd locators trained with fixed threshold, namely 0.3 and 0.5. Concretely, we notice that the training paradigm between adaptive threshold with fixed threshold are different. In fixed threshold training, there is no binary restraints, which means the confidence predictor is inclined to show higher confidence to positive samples (including negative samples). To this end, we show that the model selection under different threshold influences final results. As shown in the Fig. 7 and 8, the higher thresholds are

distributed with more uncertainty. This is because the higher threshold leaves the confidence predictor more tolerance and variance. Therefore, the scopes of two thresholds are similar but the variance are with difference.

#### D. Experimental Guarantees

1) *Convergence to DPD*: we provide some empirical guarantees on the convergence strategy to the dynamic proxy domain. Recall that the proposed strategy suggests a stronger loss function (Eq. 24), which means introduces more gradient optimization, adopted in dynamic proxy domain convergence aids crowd locator generalize well. To demonstrate the proposition empirically, we compare the convergence process under two settings. Specifically, we visualize the training curve between two settings, namely with and without strong loss in the main text, which is as shown in Fig. 9.

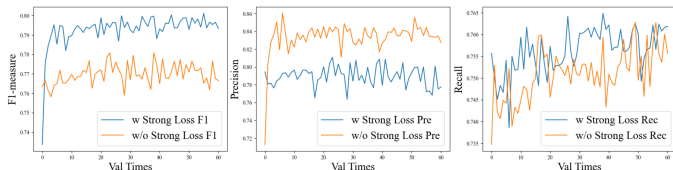


Fig. 9. The training curve between  $w$ . and  $w/o$ . strong loss.

Concretely, the model trained with strong loss is the strategy arrayed in the main text, while the model without strong loss means only  $\mathcal{L}_1$  loss is adopted. As shown in the Fig. 9, the model with stronger loss converges faster and keeps stable in the high performance. To this end, the stronger loss is indeed helpful in converging to the dynamic proxy domain and learning with more generalization.

2) *Influence Number of Samples in Gradient Descend*: In this subsection, we investigate how the number of training samples influences the final results. Theoretically, we prove that more samples within a ERM training introduces better generalization. However, in real convergence, a feasible way to improve number of samples is to enhance the batch size, which is a hyper parameters in optimization process. To this end, the issue lies in the point. In the main text, we utilize a momentum updated model to implement the first order dynamic proxy domain optimization and alleviate the issue simultaneously. Therefore, we make further analysis from the aspect of empirical results.

As shown in the Fig. 10, the curve denotes variance of metrics namely F1-measure, precision and recall for models trained under different batch size or strategy. For every setting, we pick three models, then visualize median, minimum and maximum on the boxplots. To be concrete, when the batch size is improved under tipping point, it indeed facilitates generalization. Nevertheless, a larger batch size introduces worse generalization. However, our adopted momentum training strategy only adopted number of samples which is two times than normal, which is 8 in our baseline, but we achieve a best generalization.

3) *Order for Generating DPD*: In this subsection, we empirically demonstrate the proposals shown in Thm. 1 respectively. The results are arrayed in Table. II. As shown in Table.

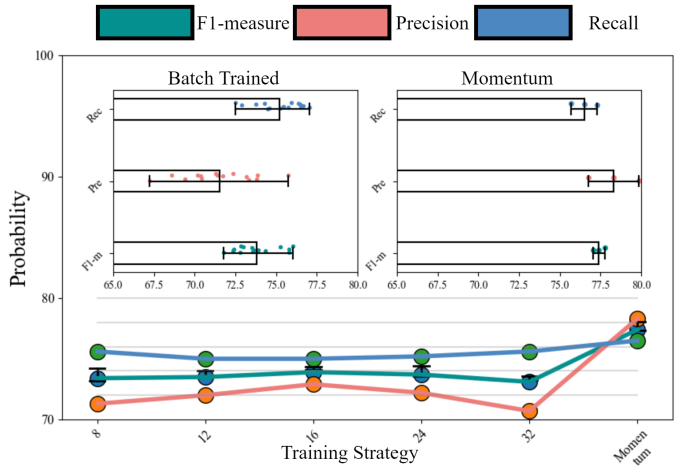


Fig. 10. Comparison of models trained under different batch size and momentum manner. We pick three trained models under one setting.

II, each component based on our theoretical guarantees also has consistent experimental guarantee. As shown, we can treat the *Multi-Crop Momentum Training* as the combination of the first order generated dynamic proxy domain with the improved number of samples, while the *Dynamic Proxy Domain* can be treat as the second order dynamic proxy domain. It is obvious that once the generation manner owns a higher order, a better result is obtained.

TABLE II  
EXPERIMENTAL GUARANTEES ON OUR PROPOSAL. EACH COMPONENT IS CORRESPONDING TO A THEORETICAL GUARANTEE.

Guarantees	F1-m (%)	Pre. (%)	Rec. (%)
Baseline Zero Order	73.4 $\pm$ 0.55	71.3 $\pm$ 0.15	75.6 $\pm$ 0.25
Multi-Crop Momentum Training	77.4 $\pm$ 0.35	78.3 $\pm$ 1.55	<b>76.5 <math>\pm</math>0.80</b>
Dynamic Proxy Domain	<b>80.1 <math>\pm</math>0.10</b>	<b>85.0 <math>\pm</math>0.60</b>	75.7 $\pm$ 0.50

TABLE III  
COMPARISON ON DPD GENERATION MANNER. THE *zero order* DENOTES THE SOURCE DOMAIN CONVERGENCE. *Input Gauss* AND *Embed Gauss* ARE AVERAGED THROUGH THREE  $\sigma$  NAMEDLY {0.1, 0.2, 0.5}.

Perturbation	F1-m (%)	Pre. (%)	Rec. (%)
Zero Order	73.4 $\pm$ 0.55	71.3 $\pm$ 0.15	75.6 $\pm$ 0.25
MC Dropout	71.3 $\pm$ 3.00	68.0 $\pm$ 4.60	75.1 $\pm$ 1.00
Color Jitter	74.3 $\pm$ 0.05	72.3 $\pm$ 0.30	<b>76.3 <math>\pm</math>0.40</b>
Embed Gauss	73.6 $\pm$ 0.55	71.1 $\pm$ 1.20	<b>76.3 <math>\pm</math>0.20</b>
Input Gauss	75.3 $\pm$ 0.25	74.4 $\pm$ 0.25	76.2 $\pm$ 0.75
Ours DPD	<b>80.1 <math>\pm</math>0.10</b>	<b>85.0 <math>\pm</math>0.60</b>	75.7 $\pm$ 0.50

4) *Generating DPD in Different Manner*: In this subsection, we exploit some other manners to generate the dynamic proxy domain. To begin with, we deem the following manners could also expand the training domain, in which the results are shown in Table. III. Intuitively, data augmentation is an usual method. However, in pixel-wise scene understanding, the to keep augmented images being consistency, only the color-jitter is implemented. What's more, some perturbations could



TABLE IV

THE MAIN RESULTS OF THE CROWD LOCALIZATION UNDER FIVE KINDS OF DOMAIN GENERALIZATION SETTINGS. ALL RESULTS ARE REPEATED THREE TIMES.

Method	SHHA to SHHB (%)			SHHA to QNRF (%)			SHHA to JHU (%)			SHHA to NWPU (%)			SHHA to FDST (%)		
	F1-m	Pre.	Rec.	F1-m	Pre.	Rec.	F1-m	Pre.	Rec.	F1-m	Pre.	Rec.	F1-m	Pre.	Rec.
Thre. 3	70.20	66.53	<b>74.29</b>	60.64	66.57	<b>56.21</b>	50.14	57.24	44.60	58.57	61.73	<b>55.72</b>	34.38	21.52	<b>85.47</b>
Thre. 5	74.69	78.44	71.29	60.01	77.55	48.94	50.86	72.11	39.28	60.01	75.47	49.81	64.51	54.51	79.00
RSC	73.92	74.75	73.11	59.23	69.00	51.88	50.77	62.18	42.90	58.11	65.62	52.14	33.71	21.20	82.06
EFDM	75.65	78.57	72.94	60.02	74.02	50.47	51.34	66.50	41.80	60.21	73.29	51.08	48.38	34.51	80.90
IRM	75.23	76.28	<u>74.22</u>	61.80	71.31	<u>54.53</u>	53.23	63.99	<b>45.57</b>	60.18	67.93	<u>54.01</u>	40.09	26.55	<u>81.88</u>
CORAL	76.43	78.87	74.14	62.45	74.39	53.81	54.38	68.31	<u>45.17</u>	61.98	74.26	53.19	60.81	48.37	81.87
IIM	75.57	78.33	73.00	61.13	74.38	51.88	51.76	66.83	42.24	61.08	74.92	51.55	62.44	51.33	79.67
OT-M	76.89	81.82	72.52	62.37	76.94	52.43	53.46	<b>72.21</b>	42.44	62.28	77.65	51.98	<u>67.48</u>	<u>58.33</u>	80.03
STEERER	<u>77.45</u>	<u>83.24</u>	72.41	<b>63.44</b>	<u>79.97</u>	<u>52.57</u>	<u>54.47</u>	71.63	43.94	<u>63.79</u>	<u>79.63</u>	53.20	66.22	56.17	80.64
DPD	<b>78.61</b>	<b>84.28</b>	73.66	<u>63.35</u>	<b>80.62</b>	52.17	<b>54.63</b>	<u>71.89</u>	44.09	<b>64.24</b>	<b>79.97</b>	53.68	<b>68.98</b>	<b>60.83</b>	79.66

also have a probability on changing the data distribution. We conduct two kinds of perturbations: (1) input perturbation, in which the input images are conducted with Gaussian noise, more specifically, we conduct three levels noise ratios; (2) intermediate perturbation, in which the intermediate representations to the images are conducted Gaussian noise, in which we conduct three levels ratios; (3) model perturbation, in which the model representation are conducted with Monte Carlo Dropout to simulate the model perturbation.

### E. Main Result

In this subsection, we compare our proposed DPD with some crowd locators adopting different thresholds. To be concrete, we set thresholds at 0.3, 0.5 and select methods like IIM [10], RSC [46], EFDM [47], IRM [48], CORAL [49], OT-M [9] and STEERER [50] for better comparisons. We notice that DPD performs well under most circumstances. As shown in the Table. IV, the adopted norms are F1-m(%), *precision* and *recall*, in which the F1-m(%) is the main metric.

Within cross-dataset scenarios, the DPD algorithm significantly outperformed other methods, particularly when addressing the SHHA to SHHB dataset. Its superior F1 score, precision, and recall rates attest to its exceptional performance on datasets with high similarity. This performance advantage may be attributed to the robust mechanisms of DPD in feature extraction and generalization, enabling it to more effectively capture and utilize commonalities across varying scenes. However, it was observed that the recall rate of DPD was marginally lower when the target domain was the FDST dataset, especially at a threshold setting of 0.3. This phenomenon could indicate a potential over-sensitivity in predicting the number of instances, leading to an increase in false positives. Furthermore, the low threshold setting might have relaxed the criteria for instance selection, enhancing the recall rate but at the cost of precision. This trade-off reflects the necessity for finer adjustments of DPD in specific contexts. Overall, DPD demonstrated exemplary performance across multiple cross-dataset scenarios, validating its robust generalization capability in the realm of domain adaptation.

## VI. CONCLUSION

In this paper, we are motivated by enhancing the generalization of crowd localization to agnostic domains. We exploit

the generalization issue from the irrationally paired thresholds and confidences. To tackle the issue, we theoretically prove introducing a dynamic proxy domain deduces the generalization error risk upper bound to target domain and experimentally propose a corresponding DPD model to demonstrate the empirical effectiveness on five domain generalization settings. To the best of our knowledge, this paper firstly makes attempt on domain generalization crowd localization. We hope this study could attract more researchers' attention on the issue.

## APPENDIX A PSEUDO CODE

### A. Data Flow for Instance Segmentation Locator

To better clarify the pipeline of adaptive threshold crowd localization, we provide a pseudo code of data flow.

---

#### Algorithm 1 Data Flow for Instance Segmentation Locator

---

**Input:** Training image  $x \in \mathbb{R}^{3 \times H \times W}$  Training binary map  $y_{gt}^b \in \mathbb{N}_{\{0,1\}}^{1 \times H \times W}$ ;  
**Input:** Encoder  $h_E$ , Decoder  $h_D$  and Threshold learner  $h_T$ .  
1: **procedure** FORWARD  
2: Feed  $x$  as input to  $h_E$ , then derive  $h_E(x) \in \mathbb{R}^{ch \times H' \times W'}$ ,  
3: For  $h_E(x)$ ,  $ch \gg 3$  and  $H' < H$ ,  $W' < W$ ;  
4: Feed  $h_E(x)$  as input to  $h_D$ , then derive  $y_{pre}^c \in \mathbb{R}^{1 \times H \times W}$ ,  
5: Feed  $h_E(x)$  as input to  $h_T$ , then derive  $y_{pre}^t \in \mathbb{R}^{1 \times H \times W}$ ,  
6: Derive  $y_{pre}^b \in \mathbb{N}_{\{0,1\}}^{1 \times H \times W}$  via  $\lceil y_{pre}^c \geq y_{pre}^t \rceil$ .  
7: **end procedure**  
8: **procedure** BACKWARD  
9: Compute loss  $\mathcal{L}$  in the main text;  
10: Update parameters according to  $\nabla g = \frac{\partial \mathcal{L}}{\partial \theta_{\{h_E, h_D, h_T\}}}$   
11: **end procedure**

---

### B. Dynamic Proxy Domain Algorithm

The pseudo code below shows our DPD training flow in detail, supplementing it with theoretical and practical inferences. Our code will be available at the url.

---

**Algorithm 2** Dynamic Proxy Domain Algorithm
 

---

**Input:** Empirical source domain  $\mathcal{S} = \{(x_i, y_i)\}_{i=1}^{N_S} \sim \mathcal{D}_s$ ;  
**Input:** Main hypothesis mapping function  $h = h_E \circ h_D \circ h_T$ ,  
 Momentum hypothesis mapping function  $h_{M_o} = h_{E_o}^{M_o} \circ h_D^{M_o} \circ h_T^{M_o}$ , Dynamic proxy domain generator  $h_T^{\mathcal{H}\Delta\mathcal{H}}$ ;  
**Input:** Empirical target domain  $\mathcal{T} = \{(x_i^t, y_i^t)\}_{i=1}^{N_t} \sim \mathcal{D}_t$ ;

- 1: **procedure** TRAIN
- 2: Initialize  $h$  and  $h_{M_o}$  with ERM on  $\mathcal{S}$
- 3: Initialize  $h_T^{\mathcal{H}\Delta\mathcal{H}}$  randomly
- 4: **for** # of gradient iterations **do**:
- 5:     Sample and crop  $(x_i, y_i)$  and  $(x_j, y_j)$  from  $\mathcal{S}$ ;
- 6:     Leverage  $h$  to predict  $y_i^c, y_j^c$ ;
- 7:     Minimize  $\mathcal{L}_{ERM}$  in Eq. 19 of the main text  
        ▷ Empirical risk minimization
- 8:     Leverage  $h$  to predict  $y_i^c, y_j^c$ ;
- 9:     Leverage  $h_{M_o}$  to infer  $y_{j(M_o)}^c, y_{j(M_o)}^b$ ;
- 10:     Minimize  $\mathcal{L}_{consis}$  in Eq. 20 of the main text  
        ▷ Multi-crop momentum
- 11:     Leverage  $h^{\mathcal{H}\Delta\mathcal{H}_T}$  to generate  $y_{j(DPD)}^b$  composing  
        dynamic proxy domain  $\mathcal{D}_p$ ,
- 12:     Minimize  $\mathcal{L}_{DPD}$  in Eq. 23 of the main text.  
        ▷ Dynamic proxy domain
- 13: **end for**
- 14: **end procedure**
- 15: **procedure** TEST
- 16: Free the parameters of  $h$ ;
- 17: **for**  $x^t$  sampled from  $\mathcal{T}$  **do**:
- 18:     Let  $h$  predict  $y_{pre}^c, y_{pre}^T$  for  $x^t$ ,
- 19:     Make binary prediction to obtain  $y_{pre}^b$  via  
         $\lceil y_{pre}^c \geq y_{pre}^T \rceil$ .
- 20: **end for**
- 21: **end procedure**

---

APPENDIX B  
PROOF TO LEMMA. 1

**Lemma 1.** Assume that the  $\mathcal{H}$  is a hypothesis space with a VC dimension of  $d$  and  $m$  is the number of training samples, drawn from  $\mathcal{D}_s$ . Given an  $h \in \mathcal{H}$ , the following inequality holds with a probability at least  $1 - \delta$ , where  $\delta \in (0, 1)$ :

$$R_{\mathcal{T}}(h) \leq \widehat{R}_{\mathcal{S}}(h) + \frac{1}{2} \widehat{d}_{\mathcal{H}\Delta\mathcal{H}}(\mathcal{S}, \mathcal{T}) + 4\sqrt{\frac{2d \log(2m) + \log(\frac{2}{\delta})}{m}} + \lambda, \quad (\text{B.27})$$

in which

$$\lambda = \inf_{\hat{h} \in \mathcal{H}} \left[ R_{\mathcal{S}}(\hat{h}) + R_{\mathcal{T}}(\hat{h}) \right]. \quad (\text{B.28})$$

**Proof:** To prove Lemma. 1, we should firstly introduce another two lemmas.

**Lemma 2.** Assume  $\mathcal{H}$  is a hypothesis space with a VC dimension of  $d$ . Let  $\mathcal{S}$  with  $\mathcal{D}$  are empirically sampled based

on i.i.d. from  $\mathcal{D}_s$  with  $\mathcal{D}_t$  respectively. Then we have Eq. B.29 holds with a probability at least  $1 - \delta$  for any  $\delta \in (0, 1)$ :

$$d_{\mathcal{H}\Delta\mathcal{H}}(\mathcal{D}_s, \mathcal{D}_t) \leq \widehat{d}_{\mathcal{H}\Delta\mathcal{H}}(\mathcal{S}, \mathcal{T}) + 4\sqrt{\frac{d \log(2m) + \log(\frac{2}{\delta})}{m}} \quad (\text{B.29})$$

**Lemma 3.** Let  $\hat{h}, h$  be any hypothesis function defined on  $\mathcal{H}$ , we have Eq. B.30 holds.

$$|R_{\mathcal{S}}(h, h') - R_{\mathcal{T}}(h, h')| \leq \frac{1}{2} d_{\mathcal{H}\Delta\mathcal{H}}(\mathcal{D}_s, \mathcal{D}_t). \quad (\text{B.30})$$

As for the proof to Lemma 2 and 3, please refer to [51]. Finally, we are ready to prove Lemma. 1. To begin with, according to the triangle inequality, we start from:

$$\begin{aligned} R_{\mathcal{T}}(h) &\leq R_{\mathcal{T}}(\hat{h}) + R_{\mathcal{T}}(\hat{h}, h) \\ &\leq \left| R_{\mathcal{T}}(h, \hat{h}) - R_{\mathcal{S}}(h, \hat{h}) \right| + R_{\mathcal{T}}(\hat{h}) + R_{\mathcal{S}}(h, \hat{h}) \\ &\leq R_{\mathcal{T}}(\hat{h}) + R_{\mathcal{S}}(h, \hat{h}) + \frac{1}{2} d_{\mathcal{H}\Delta\mathcal{H}}(\mathcal{D}_s, \mathcal{D}_t) \\ &\leq R_{\mathcal{T}}(\hat{h}) + R_{\mathcal{S}}(h) + R_{\mathcal{S}}(\hat{h}) + \frac{1}{2} d_{\mathcal{H}\Delta\mathcal{H}}(\mathcal{D}_s, \mathcal{D}_t) \\ &\leq R_{\mathcal{S}}(h) + \frac{1}{2} \widehat{d}_{\mathcal{H}\Delta\mathcal{H}}(\mathcal{S}, \mathcal{T}) \\ &\quad + 4\sqrt{\frac{2d \log(2m) + \log(\frac{2}{\delta})}{m}} + \lambda. \end{aligned} \quad (\text{B.31})$$

APPENDIX C  
DATASETS

To further show the main statistic information and the domain shift existing among them, we array some main features of the datasets and the results are as follows.

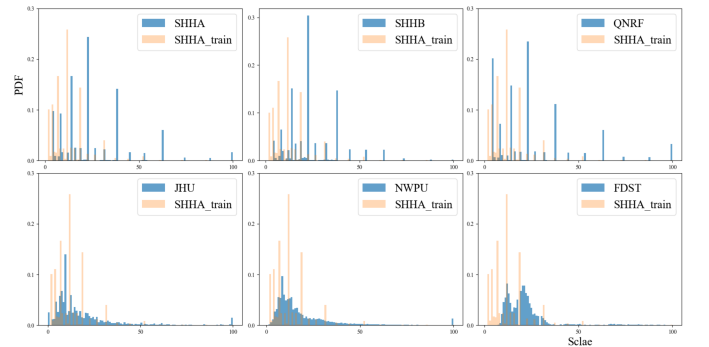


Fig. 11. Scale distribution comparison between SHHA with other adopted datasets.

TABLE V  
MAIN STATISTIC INFORMATION ON THE SIX ADOPTED DATASETS

Dataset	Set Count	Avg. Count	Avg. Resolution
SHHA	241,677	501	589*868
SHHB	88,488	123	768*1024
QNRF	1,251,642	815	2013*2902
JHU	1,515,005	346	1430*910
NWPU	2,133,375	418	2191*3209
FDST	394,081	27	1080*1920

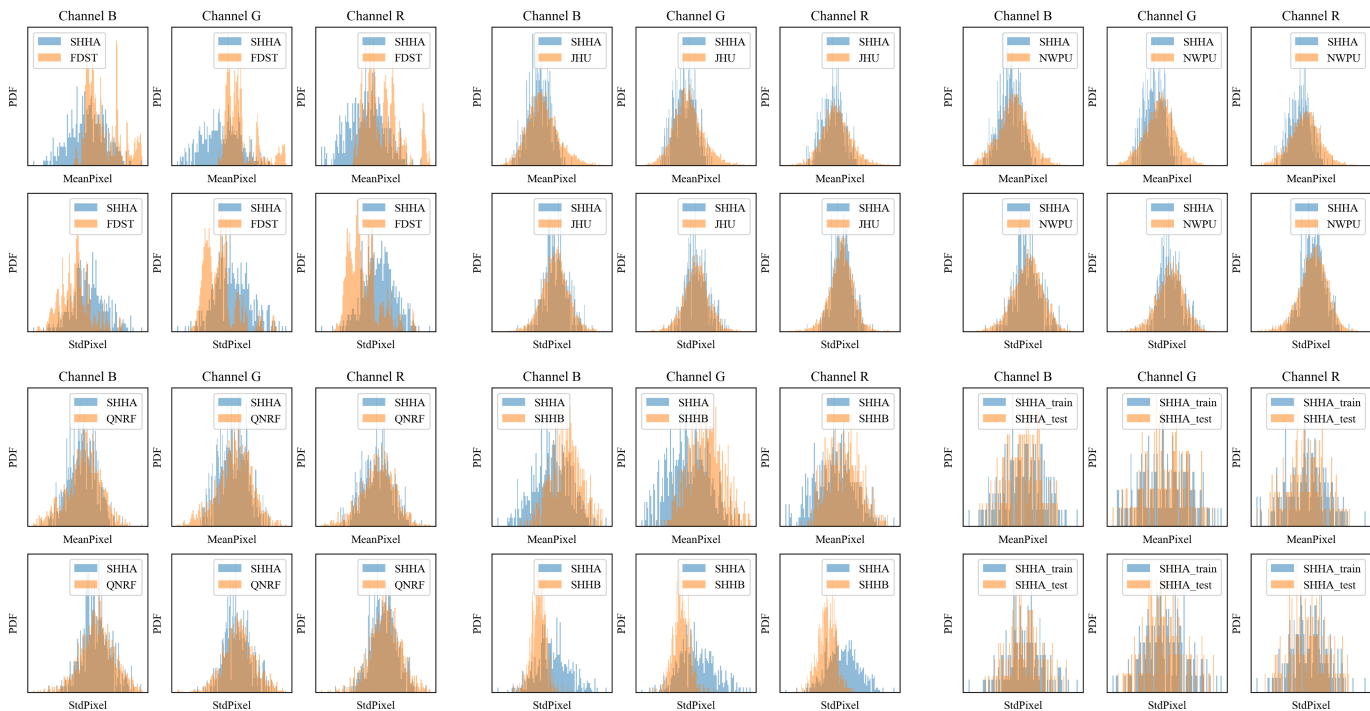


Fig. 12. Scene distribution comparison between SHHA with other datasets. Concretely, the scene distribution can be decoupled into the statistics namely mean and standard deviation for pixel values in RGB channels.

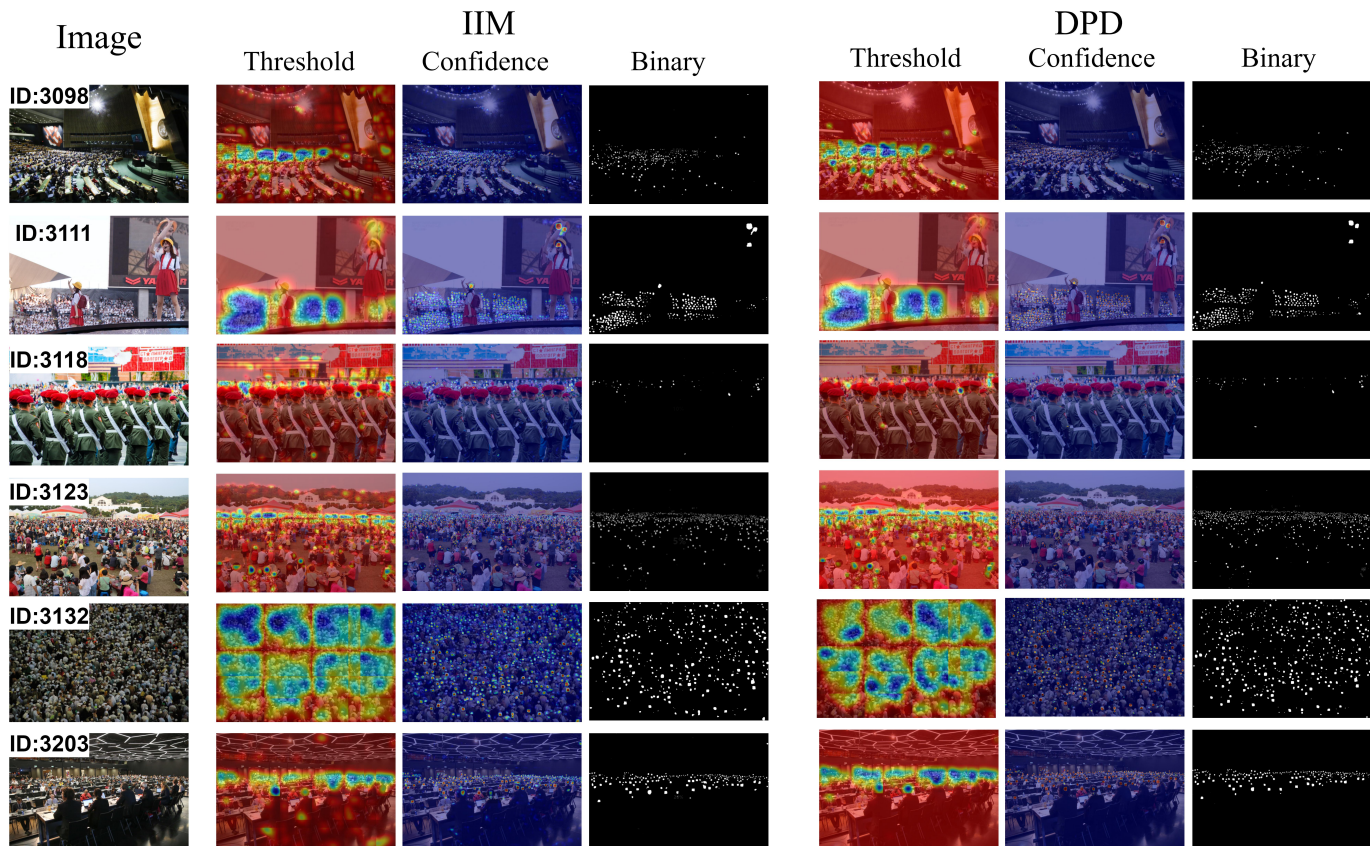


Fig. 13. Some typical visualization results from NWPU-Crowd validation set.

## REFERENCES

- [1] J. Gao, T. Han, Y. Yuan, and Q. Wang, "Domain-adaptive crowd counting via high-quality image translation and density reconstruction," *IEEE transactions on neural networks and learning systems*, vol. 34, no. 8, pp. 4803–4815, 2021.
- [2] D. Liang, W. Xu, Y. Zhu, and Y. Zhou, "Focal inverse distance transform maps for crowd localization," *IEEE Transactions on Multimedia*, 2022.
- [3] J. Wang, J. Gao, Y. Yuan, and Q. Wang, "Crowd localization from gaussian mixture scoped knowledge and scoped teacher," *IEEE Transactions on Image Processing*, vol. 32, pp. 1802–1814, 2023.
- [4] J. Gao, M. Gong, and X. Li, "Congested crowd instance localization with dilated convolutional swin transformer," *Neurocomputing*, vol. 513, pp. 94–103, 2022.
- [5] H. Zhu, J. Yuan, X. Zhong, Z. Yang, Z. Wang, and S. He, "Daot: Domain-agnostically aligned optimal transport for domain-adaptive crowd counting," in *Proceedings of the 31st ACM International Conference on Multimedia*, 2023, pp. 4319–4329.
- [6] P. Ge, C.-X. Ren, X.-L. Xu, and H. Yan, "Unsupervised domain adaptation via deep conditional adaptation network," *Pattern Recognition*, vol. 134, p. 109088, 2023.
- [7] H. Xie, Z. Yang, H. Zhu, and Z. Wang, "Striking a balance: Unsupervised cross-domain crowd counting via knowledge diffusion," in *Proceedings of the 31st ACM International Conference on Multimedia*, 2023, pp. 6520–6529.
- [8] S. Abousamra, M. Hoai, D. Samaras, and C. Chen, "Localization in the crowd with topological constraints," in *Proceedings of the AAAI Conference on Artificial Intelligence*, vol. 35, no. 2, 2021, pp. 872–881.
- [9] W. Lin and A. B. Chan, "Optimal transport minimization: Crowd localization on density maps for semi-supervised counting," in *Proceedings of the IEEE/CVF Conference on Computer Vision and Pattern Recognition*, 2023, pp. 21 663–21 673.
- [10] J. Gao, T. Han, Q. Wang, Y. Yuan, and X. Li, "Learning independent instance maps for crowd localization," *arXiv preprint arXiv:2012.04164*, 2020.
- [11] D. Liang, J. Xie, Z. Zou, X. Ye, W. Xu, and X. Bai, "Crowdclip: Unsupervised crowd counting via vision-language model," in *Proceedings of the IEEE/CVF Conference on Computer Vision and Pattern Recognition*, 2023, pp. 2893–2903.
- [12] W. Zhou, X. Yang, J. Lei, W. Yan, and L. Yu, "Mc<sup>3</sup>net: Multimodality cross-guided compensation coordination network for rgb-t crowd counting," *IEEE Transactions on Intelligent Transportation Systems*, 2023.
- [13] Q. Zhang and A. B. Chan, "Calibration-free multi-view crowd counting," in *European Conference on Computer Vision*. Springer, 2022, pp. 227–244.
- [14] H. Lin, Z. Ma, X. Hong, Y. Wang, and Z. Su, "Semi-supervised crowd counting via density agency," in *Proceedings of the 30th ACM International Conference on Multimedia*, 2022, pp. 1416–1426.
- [15] D. Liang, X. Chen, W. Xu, Y. Zhou, and X. Bai, "Transcrowd: weakly-supervised crowd counting with transformers," *Science China Information Sciences*, vol. 65, no. 6, p. 160104, 2022.
- [16] J. Wan and A. Chan, "Modeling noisy annotations for crowd counting," *Advances in Neural Information Processing Systems*, vol. 33, pp. 3386–3396, 2020.
- [17] J. Redmon, S. Divvala, R. Girshick, and A. Farhadi, "You only look once: Unified, real-time object detection," in *Proceedings of the IEEE conference on computer vision and pattern recognition*, 2016, pp. 779–788.
- [18] S. Ren, K. He, R. Girshick, and J. Sun, "Faster r-cnn: Towards real-time object detection with region proposal networks," *Advances in neural information processing systems*, vol. 28, 2015.
- [19] P. Hu and D. Ramanan, "Finding tiny faces," in *Proceedings of the IEEE conference on computer vision and pattern recognition*, 2017, pp. 951–959.
- [20] Y. Bai, Y. Zhang, M. Ding, and B. Ghanem, "Finding tiny faces in the wild with generative adversarial network," in *Proceedings of the IEEE conference on computer vision and pattern recognition*, 2018, pp. 21–30.
- [21] Z. Li, X. Tang, J. Han, J. Liu, and R. He, "Pyramidbox++: High performance detector for finding tiny face," *arXiv preprint arXiv:1904.00386*, 2019.
- [22] Q. Song, C. Wang, Z. Jiang, Y. Wang, Y. Tai, C. Wang, J. Li, F. Huang, and Y. Wu, "Rethinking counting and localization in crowds: A purely point-based framework," in *Proceedings of the IEEE/CVF International Conference on Computer Vision*, 2021, pp. 3365–3374.
- [23] X. Yu, P. Chen, D. Wu, N. Hassan, G. Li, J. Yan, H. Shi, Q. Ye, and Z. Han, "Object localization under single coarse point supervision," in *Proceedings of the IEEE/CVF Conference on Computer Vision and Pattern Recognition*, 2022, pp. 4868–4877.
- [24] H. Li, L. Liu, K. Yang, S. Liu, J. Gao, B. Zhao, R. Zhang, and J. Hou, "Video crowd localization with multifocus gaussian neighborhood attention and a large-scale benchmark," *IEEE Transactions on Image Processing*, vol. 31, pp. 6032–6047, 2022.
- [25] J. Wen, R. Liu, N. Zheng, Q. Zheng, Z. Gong, and J. Yuan, "Exploiting local feature patterns for unsupervised domain adaptation," in *Proceedings of the AAAI conference on artificial intelligence*, vol. 33, no. 01, 2019, pp. 5401–5408.
- [26] J. Wen, N. Zheng, J. Yuan, Z. Gong, and C. Chen, "Bayesian uncertainty matching for unsupervised domain adaptation," *arXiv preprint arXiv:1906.09693*, 2019.
- [27] Y. Zhang, T. Liu, M. Long, and M. Jordan, "Bridging theory and algorithm for domain adaptation," in *International conference on machine learning*. PMLR, 2019, pp. 7404–7413.
- [28] Y. Ganin, E. Ustinova, H. Ajakan, P. Germain, H. Larochelle, F. Laviolette, M. March, and V. Lempitsky, "Domain-adversarial training of neural networks," *Journal of machine learning research*, vol. 17, no. 59, pp. 1–35, 2016.
- [29] W. Liu, N. Durasov, and P. Fua, "Leveraging self-supervision for cross-domain crowd counting," in *Proceedings of the IEEE/CVF Conference on Computer Vision and Pattern Recognition*, 2022, pp. 5341–5352.
- [30] Q. Wang, T. Han, J. Gao, and Y. Yuan, "Neuron linear transformation: Modeling the domain shift for crowd counting," *IEEE Transactions on Neural Networks and Learning Systems*, vol. 33, no. 8, pp. 3238–3250, 2021.
- [31] H. Zhu, J. Yuan, Z. Yang, X. Zhong, and Z. Wang, "Fine-grained fragment diffusion for cross domain crowd counting," in *Proceedings of the 30th ACM International Conference on Multimedia*, 2022, pp. 5659–5668.
- [32] Z. Zou, X. Qu, P. Zhou, S. Xu, X. Ye, W. Wu, and J. Ye, "Coarse to fine: Domain adaptive crowd counting via adversarial scoring network," in *Proceedings of the 29th ACM International Conference on Multimedia*, 2021, pp. 2185–2194.
- [33] Z. Du, J. Deng, and M. Shi, "Domain-general crowd counting in unseen scenarios," in *Proceedings of the AAAI Conference on Artificial Intelligence*, vol. 37, no. 1, 2023, pp. 561–570.
- [34] Q. Wu, J. Wan, and A. B. Chan, "Dynamic momentum adaptation for zero-shot cross-domain crowd counting," in *Proceedings of the 29th ACM International Conference on Multimedia*, 2021, pp. 658–666.
- [35] S. Ben-David, J. Blitzer, K. Crammer, and F. Pereira, "Analysis of representations for domain adaptation," *Advances in neural information processing systems*, vol. 19, 2006.
- [36] J. Cha, S. Chun, K. Lee, H.-C. Cho, S. Park, Y. Lee, and S. Park, "Swad: Domain generalization by seeking flat minima," *Advances in Neural Information Processing Systems*, vol. 34, pp. 22 405–22 418, 2021.
- [37] Y. Zhang, D. Zhou, S. Chen, S. Gao, and Y. Ma, "Single-image crowd counting via multi-column convolutional neural network," in *Proceedings of the IEEE conference on computer vision and pattern recognition*, 2016, pp. 589–597.
- [38] H. Idrees, M. Tayyab, K. Athrey, D. Zhang, S. Al-Maadeed, N. Rajpoot, and M. Shah, "Composition loss for counting, density map estimation and localization in dense crowds," in *Proceedings of the European conference on computer vision (ECCV)*, 2018, pp. 532–546.
- [39] V. A. Sindagi, R. Yasarla, and V. M. Patel, "Pushing the frontiers of unconstrained crowd counting: New dataset and benchmark method," in *Proceedings of the IEEE/CVF International Conference on Computer Vision*, 2019, pp. 1221–1231.
- [40] Q. Wang, J. Gao, W. Lin, and X. Li, "Nwpu-crowd: A large-scale benchmark for crowd counting and localization," *IEEE transactions on pattern analysis and machine intelligence*, vol. 43, no. 6, pp. 2141–2149, 2020.
- [41] Y. Fang, B. Zhan, W. Cai, S. Gao, and B. Hu, "Locality-constrained spatial transformer network for video crowd counting," in *2019 IEEE international conference on multimedia and expo (ICME)*. IEEE, 2019, pp. 814–819.
- [42] J. Gao, W. Lin, B. Zhao, D. Wang, C. Gao, and J. Wen, "C<sup>3</sup> framework: An open-source pytorch code for crowd counting," *arXiv preprint arXiv:1907.02724*, 2019.
- [43] K. Simonyan and A. Zisserman, "Very deep convolutional networks for large-scale image recognition," *arXiv preprint arXiv:1409.1556*, 2014.
- [44] T.-Y. Lin, P. Dollár, R. Girshick, K. He, B. Hariharan, and S. Belongie, "Feature pyramid networks for object detection," in *Proceedings of the IEEE conference on computer vision and pattern recognition*, 2017, pp. 2117–2125.



- [45] D. P. Kingma and J. Ba, “Adam: A method for stochastic optimization,” *arXiv preprint arXiv:1412.6980*, 2014.
- [46] Z. Huang, H. Wang, E. P. Xing, and D. Huang, “Self-challenging improves cross-domain generalization,” in *Computer vision–ECCV 2020: 16th European conference, Glasgow, UK, August 23–28, 2020, proceedings, part II 16*. Springer, 2020, pp. 124–140.
- [47] Y. Zhang, M. Li, R. Li, K. Jia, and L. Zhang, “Exact feature distribution matching for arbitrary style transfer and domain generalization,” in *Proceedings of the IEEE/CVF conference on computer vision and pattern recognition*, 2022, pp. 8035–8045.
- [48] M. Arjovsky, L. Bottou, I. Gulrajani, and D. Lopez-Paz, “Invariant risk minimization,” *arXiv preprint arXiv:1907.02893*, 2019.
- [49] B. Sun and K. Saenko, “Deep coral: Correlation alignment for deep domain adaptation,” in *Computer Vision–ECCV 2016 Workshops: Amsterdam, The Netherlands, October 8–10 and 15–16, 2016, Proceedings, Part III 14*. Springer, 2016, pp. 443–450.
- [50] T. Han, L. Bai, L. Liu, and W. Ouyang, “Steerer: Resolving scale variations for counting and localization via selective inheritance learning,” in *Proceedings of the IEEE/CVF International Conference on Computer Vision*, 2023, pp. 21 848–21 859.
- [51] S. Ben-David, J. Blitzer, K. Crammer, A. Kulesza, F. Pereira, and J. W. Vaughan, “A theory of learning from different domains,” *Machine learning*, vol. 79, pp. 151–175, 2010.